Pharmacological modulation of LMNA SRSF1-dependent splicing abrogates diet-induced obesity in mice

Julien Santo, Célia Lopez-Herrera, Cécile Apolit, Yacine Bareche, Laure Lapasset, Carine Chavey, Serena Capozi, Florence Mahuteau, Romain Najman, Pauline Fornarelli, et al.

Pharmacological modulation of LMNA SRSF1-dependent splicing abrogates diet-induced obesity in mice

J Santo, C Lopez-Herrera, C Apolit, Y Bareche, L Lapasset, C Chavey, S Capozi, F Mahuteau, R Najman, P Fornarelli, I C Lopez-Mejía, G Béranger, F Casas, E-Z Amri, B Pau, D Scherrer, J Tazi

Cite this article as: J Santo, C Lopez-Herrera, C Apolit, Y Bareche, L Lapasset, C Chavey, S Capozi, F Mahuteau, R Najman, P Fornarelli, I C Lopez-Mejía, G Béranger, F Casas, E-Z Amri, B Pau, D Scherrer, J Tazi, Pharmacological modulation of LMNA SRSF1-dependent splicing abrogates diet-induced obesity in mice, *International Journal of Obesity* accepted article preview 5 December 2016; doi: 10.1038/ijo.2016.220.

Received 4 July 2016; revised 26 October 2016; accepted 1 November 2016; Accepted article preview online 5 December 2016

Title: Pharmacological Modulation of LMNA SRSF1-dependent Splicing Abrogates Diet-Induced Obesity in Mice

Julien Santo[1, †], Celia Lopez-Herrera[1, †], Cécile Apolit[1, †], Yacine Bareche[2], Laure Lapasset[1], Carine Chavey[2], Serena Capozi[2], Florence Mahuteau[3], Romain Najman[1, 3], Pauline Fornarelli[1, 3], Isabel C. Lopez-Mejía[2], Guillaume Béranger[6], François Casas[5], Ez-Zoubir Amri[6], Bernard Pau[4], Didier Scherrer[1], and Jamal Tazi[2]*

1) ABIVAX, 1919 Route de Mende, 34293 Montpellier Cedex 5, France.

2) Institut de Génétique Moléculaire de Montpellier, CNRS UMR 5535, 1919 Route de Mende, 34293 Montpellier Cedex 5, University of Montpellier, France.

3) Institut Curie, UMR176, Bâtiment 110, Centre Universitaire 91405 Orsay Cedex, France.

4) Université de Montpellier, UFR Pharmacie, 15 Avenue Charles Flahault, 34000 Montpellier, France.

5) UMR Dynamique Musculaire et Métabolisme, INRA - CAMPUS SUPAGRO 2 place Viala 34060 Montpellier Cedex 2, France.

6) Institut de Biologie de Valrose, UMR CNRS 7277 – UMR INSERM 1091, Université de Nice Sophia Antipolis, Faculté de Médecine, 28 Avenue de Valombrose, 06107 Nice Cedex 2, France.

† These authors contributed equally to this work.

* **Corresponding author:** E-mail: jamal.tazi@igmm.cnrs.fr

Short title: ABX300 as a new drug for obesity treatment

Abstract

Bakground/objectives:

Intense drug discovery efforts in the metabolic field highlight the need for novel strategies for the treatment of obesity**.** Alternative splicing (AS) and/or polyadenylation enable the LMNA gene to express distinct protein isoforms that exert opposing effects on energy metabolism and lifespan. Here we aimed to use the splicing factor SRSF1 that contribute to the production of these different isoforms as a target to uncover new anti-obesity drug.

Subjects/Methods:

Small molecules modulating SR protein activity and splicing, were tested for their abilities to interact with SRSF1 and to modulate LMNA (AS). Using an LMNA luciferase reporter we selected molecules that were tested in Diet Induced Obese (DIO) mice. Transcriptomic analyses were performed in the white adipose tissues from untreated and treated DIO mice and mice fed a chow diet.

Results:

We identified a small molecule that specifically interacted with the RS domain of SRSF1. ABX300 abolished diet induced obesity (DIO) in mice, leading to restoration of adipose tissue homeostasis. In contrast, ABX300 had no effect on mice fed a standard chow diet. A global transcriptomic analysis revealed similar profiles of White adipose tissue (WAT) from DIO mice treated with ABX300 and from untreated mice fed a chow diet. Mice treated with ABX300 exhibited an increase in O_2 consumption and a switch in fuel preference toward lipids.

Conclusions :

Targeting SRSF1 with ABX300 compensates for changes in RNA biogenesis induced by fat accumulation and consequently represents a novel unexplored approach for the treatment of obesity.

Introduction

Obesity, defined as an imbalance of income and expenditure of energy, is a rapidly growing epidemic worldwide. Obesity is characterized by increased fat mass due to energy storage in WAT. In addition, obesity is associated with a collection of clinical problems known as the metabolic syndrome, including insulin resistance, diabetes, cardio-vascular disease, dyslipidemia, and fatty liver [1]. Owing to changes in the diet in Western countries and an increasingly "aged" population, metabolic syndrome is an epidemic expected to double in incidence in the near future [2]. Dietary management and exercise are not usually successful as an intervention, underscoring the need for efficient medication to treat metabolic disorders [3]. Integrated metabolic networks, which are governed at the transcriptional level by transcription factors and co-regulators, enable the organism to adapt the metabolic state of different organs based on nutrient availability [4]. The limited success to date in the pharmacotherapy of obesity likely reflects the existence of multiple redundant and compensatory pathways in energy homeostasis [5]. Intense drug discovery efforts in the metabolic field highlight the need for novel strategies for the treatment of obesity. Compelling data suggest that targeting cellular bioenergetics may provide an exciting new therapeutic approach for the treatment or prevention of this disorder [6].

RNA processing of the LMNA gene was recently reported to generate different isoforms with opposing effects on the energy expenditure (EE) and lifespan of mice [7]. The alternative RNA processing of *LMNA* pre-mRNA produces three nuclear protein isoforms: lamin A, progerin, and lamin C. Mutations in lamin A/C can cause several syndromes collectively described as laminopathies, which include several lipodystrophies and progeroid syndromes [8]. The lipodystrophy mutations strongly suggest that lamins can have cell-type-specific functions [9]. Moreover, a *de novo* silent mutation in *LMNA* (c.1824C>T; p.Gly608Gly) results in the aberrant AS of the lamin-A isoform, which gives rise to a truncated isoform of the protein termed progerin [10]. The exacerbated accumulation of progerin is the predominant cause of Hutchinson-Gilford Progeria Syndrome (HGPS), a severe form of early-onset premature aging associated with lipodystrophy [11,12]. In HGPS, a loss of adipose tissue correlates with

adipokine dysregulation, insulin resistance, and atherosclerosis, suggesting a critical role of adipose tissue function in controlling whole-body energy metabolism, age-related pathologies, and longevity [13]. The lamin-C isoform lacking the C-terminal domain of Lamin A and progerin acts as an antagonist that promotes fat accumulation and longevity [7].

Three serine-arginine (SR)-rich proteins of the SR protein family, namely SRSF1, SRSF5 and SRSF6, contribute to *LMNA* AS [14,15]. These splicing factors are known to bind sequences in exons called exonic splicing enhancers (ESE) and thereby activate splicing [16]. Given the described antagonistic functions of the LMNA isoforms on EE, SR proteins appear to be suitable targets of study to identify compounds for the treatment of metabolic disorders, such as obesity. In recent years, we have demonstrated that small molecules that target SR proteins selectively inhibit ESE-dependent splicing and influence the splicing efficiency of target pre-mRNAs [17-19]. Using a luciferase based-reporter to screen for small-molecule modulators of LMNA AS, we herein report that ABX300, a molecule that interacts with SRSF1, abolishes high-fat diet-induced obesity in mice. ABX300 treatment enhances energy expenditure, providing a new unexplored therapeutic approach for the treatment of obesity disorders.

Materials and Methods

Luminescence assay

HEK-293 FRT-LMNA-Luc cells were seeded 48 h prior to luminescence lecture at 10,000 cells per well. The culture medium was then removed, and the cells were washed once with sterile DPBS. The cells were lysed using 1X Passive Lysis Buffer (E1941, Promega, Madison, WI, United States), which was directly added to the cells. Half of the cell lysate was then mixed with Luciferase Assay Reagent (E1501, Promega, Madison, WI, United States), and the luciferase activity in each well was measured within 1 second. The remaining cell lysate was used for protein normalization in the well (Pierce™ 660 nm Protein Assay Reagent).

Immunofluorescence analysis

SRSF1-GFP HeLa cells were maintained in Dulbecco's modified Eagle's medium (DMEM, Invitrogen) containing 10% heat-inactivated fetal bovine serum (FBS, PAA), 2 mM L-Glutamine, and 1% penicillin and streptomycin (all from Thermo Fisher) and untreated (DMSO), treated with 5 µM of either ABX300 or ABX460. The cells were fixed in 4% (w/v) paraformaldehyde for 20 min. The nuclei were stained with Hoechst 33342 (Sigma). The cells were washed in PBS and water, mounted with DAKO mounting medium, and observed under a fluorescence microscope. Cell imaging was performed with a confocal Leica SP5-SMD. The images were processed using the FiJi software.

Fluorimetric titrations

The fluorimetric titrations were performed at a constant dye concentration (ABX300) (1.2 µM) with increasing concentrations of SRSF1 in 0.6 mM guanidine buffer (up to 120 µM). The fluorescence spectra were recorded on a FluoroMax-3 (Jobin Yvon) at room temperature. The measurements were performed with solutions of OD <0.1 to avoid reabsorption of the emitted light, and the data were corrected with a blank and based on variations in the detector with the emitted wavelength. The binding curves were obtained by plotting the fluorescence enhancement F/F0 (F= integrated fluorescence area of

the complex and F0 = integrated fluorescence area of the free dye) versus the concentration of SRSF1.

Animals and ethics statement

All animal procedures were executed according to European Directive 2010/63/UE. The mice were maintained under pathogen-free conditions in our animal facility (E34-172-16), and the experiments were conducted by authorized personnel. The study plan was approved by the Institutional Review Board at the Animal Facility of the Institut de Génétique Moléculaire de Montpellier and the Regional Ethics Committee for Animal Experimentation of Languedoc-Roussillon (agreement n° CEEA-LR-1061).

Animal feeding and treatment

Six-week-old male C57BL/6J mice were purchased from Charles River Laboratory (69592 L'Arbresle) and housed under a normal light cycle (12 h light-dark) and a constant temperature of 22°C, with free access to food and water. The experiments began after one week of acclimatization to our installations under CD conditions. At this point, mice either continued to receive the CD (Safe, 3% energy from fat) or were switched to an HFD (Research Diet 58Y1, 60% energy from fat). For the curative scheme, mice were fed for up to ten weeks to generate the DIO model and were then treated with the text compound. The mice were weighed weekly, and food intake was measured four times per week. For the preventive scheme, the treatment started along with HFD feeding. For both nourishment conditions, the mice were divided into 2 groups of treatment: half of the mice received the vehicle (Labrafil M1944CS – 5% DMSO), and the other half received the active compound ABX300 at 50 mg/kg. For both conditions the selected route of administration was intragastric to accurately manage the delivered dose.

Synchronized pair-feeding test

DIO mice were divided into three groups and housed by experimental class. HFD untreated and ABX300-treated animals were provided ad libitum access to food, whereas in the untreated pair-fed (PF) group, the food was calorie restricted. These animals received the same amount of aliment consumed by

the ABX300 treated group during the preceding 24 h. The body weights were registered twice per week.

Organ collection

After one month of treatment, the mice were anesthetized by intraperitoneal injection (xylazine/ketamine combination) and euthanized by cervical dislocation. The organs were collected, rapidly weighed and immediately snap-frozen in liquid nitrogen or fixed in 4% paraformaldehyde.

Histological analysis

Organs fixed in 4% paraformaldehyde were dehydrated, embedded in paraffin and stained with HE for histological analysis. The slides were scanned with the NanoZoomer equipment (HAMAMATSU). Virtual slides were analyzed with the NDP.view software and Image J, and the MRI Adipocyte Tool was used to measure the size of WAT cells.

Micro-computed tomography

Adipose tissue quantification was performed with a SkyScan-1178 X-ray micro-computed tomography system as previously described (Lopez-Mejia et al, 2014).

Total RNA extraction

To extract total RNA, 30 mg of WAT was ground in liquid nitrogen, and the powder was dissolved in TRI reagent (SIGMA) according to the manufacturer's protocol, followed by DNAse digestion and phenol-chloroform-isoamyl alcohol purification. The RNA quantity and integrity were controlled using a Nanodrop ND-1000 (Thermo Scientific) and an Agilent Bioanalyzer (Agilent Technologies), respectively.

miRNA array experiments

Small non-coding RNA transcripts were assessed using an Affymetrix assay, in which RNA was hybridized to Affymetrix miRNA v3.0 arrays (GenoSplice- Evry- France).

Mitochondrial target prediction analysis

Putative miRNA targets were identified using the mirDB online database (http://mirdb.org/miRDB/), which is a database for miRNA target prediction and functional annotations. Targets are predicted by an algorithm (MirTarget) that analyzes all NCBI RefSeq 3'-UTRs in order to predict both conserved and non-conserved target motifs. A target prediction score is also computed to inform the user about the confidence of the prediction. The range is from 50 to 100, but caution is recommended for values below 80. Because the microarray analysis was based on a previous version of mirBase (http://www.mirbase.org/) (v.17), the selected miRNA names were updated based on the current mirBase version (v.21). The miRNAs were then compared against the mirDB database in order to retrieve all predicted targets with a prediction score $\geq$ 80. Using the MitoCarta database (https://www.broadinstitute.org/pubs/MitoCarta/), the selected target genes were then filtered in order to exclusively retrieve specific mitochondrial target genes. The two heat maps presented in Figures 5 A and B were generated using a custom R script (https://cran.r-project.org/) containing gplots (https://cran.r-project.org/web/packages/gplots/gplots.pdf). The data were clustered using the Pearson correlation co-efficient method and the Heatmap2 function (http://www.inside-r.org/packages/cran/gplots/docs/heatmap.2).

Reverse-transcription and PCR

One microgram of RNA was reverse-transcribed using the First-strand cDNA Synthesis Kit (GE Healthcare) according to the manufacturer's instructions. Gene expression was assessed by PCR using Platinum Taq DNA Polymerase. The reactions consisted of the following: PCR buffer 1x, $MgCl_2$ 1.5 mM, primers forward and reverse 0.6 µM of each, dNTP 0.25 mM of each, Platinum Taq DNA Polymerase 2 U/rxn, 1 µl of cDNA and nuclease-free water to a final volume of 50 µl (# 10966-034 Life Technologies). PCR was performed using a Roche ThermoCycler (2 min at 94°C, 35 cycles of 30 sec 94°C/30 sec 55°C/1 min 72°C, and then 2 min at 72°C). The PCR products were analyzed with an Elmer Perkin Caliper.

Metabolic chamber experiments

DIO mice were switched to ad libitum CD feeding one week before the metabolic chamber experiments. Single-housed animals were allowed to acclimate for 24 h prior to recording. Immediately before the run, the animals were weighed and treated. Oxygen consumption (VO_2) and carbon dioxide production (VCO_2) were monitored every 2 min over a 24-h period using a Comprehensive Lab Animal Monitoring System (Columbus Instruments, Columbus, OH) controlled at 22°C. The RER corresponds to the VCO_2/VO_2 ratio.

Statistical analysis

All results are expressed as the mean +/− standard error mean (S.E.M) or standard deviation (SD). The significance of differences was determined with the appropriate statistical test, including Student's t test, Mann-Whitney test, analysis of variance (ANOVA) or Kruskal-Wallis test, with significance at * P<0.05, **P<0.01, ***P<0.001, and ****P<0.0001.

Results

Identification of ABX300

Based on the IDC16 structure, an indole derivative that specifically targets the SR protein SRSF1 and inhibits HIV multiplication *in vitro* [18], a new library was developed by ABIVAX to assess the toxic effect of IDC16 owing to its planar structure. Derivatives with quinoxaline and quinoline backbones were synthesized in order to disrupt the planar structure of IDC16 (**Fig. S1A**). The interaction of IDC16 with SRSF1 required its carboxyl-terminal serine-arginine-rich (RS) domain, which is involved in the ESE-dependent splicing activity and the localization of SRSF1. To avoid the selection of molecules that would generally affect AS because of SRSF1 mislocalization, CRISPR-edited HeLa cells expressing an endogenous GFP-SRSF1 fusion protein were used to select molecules that did not disturb the GFP distribution (**Fig. 1A**). After the elimination of all molecules that induced the mislocalization of SRSF1, a primary screen was conducted with 5 µM of each selected molecule, which was added in triplicate to an HEK-293FRT reporter cell line (HEK-293FRT-LMNA-Luc) stably expressing luciferase fused with a portion of the LMNA gene under the control of the CMV promoter (**Fig. 1B**). This cell line contained the main mutation responsible for HGPS (c.1824C>T; p.Gly608Gly) and was consequently used as a reporter for the specific use of the *LMNA* exon 11 5' splice sites (5'SS); the authentic 5' splice site produces Lamin A, and the progerin 5' splice produces progerin, and both sites are under the control of SRSF1, as previously mentioned. In this assay, the inhibition of SRSF1 should lead to the selection of an authentic splice site [14] and a consequent increase in luciferase activity.

LMNA isoforms have been shown to play important opposite roles in the regulation of the metabolic adaptations of adipose tissue in mammals. Therefore, in a secondary screen, selected molecules representative of different structures were tested for their ability to induce weight changes in high-fat diet-induced obese mice (**Fig. S1B**). Among the 22 molecules tested, one lead compound, ABX300, was identified. The binding of ABX300 to SRSF1 was determined using the intrinsic fluorescence of the drug, following a classical fluorimetric titration protocol. **Figure 1C** shows that

increasing concentrations of SRSF1 enhanced the ABX300 fluorescence, demonstrating a direct interaction between SRSF1 and ABX300 with a stoichiometric ratio of 1:1. As a negative control, we used hnRNPK protein, which does not bind to ABX300 (**Fig. S1C**). To examine the potential requirement of the RS domain for ABX300 binding, we used mutant protein in which the entire C-terminal RS domain was deleted. No binding was observed with the mutant protein, indicating that the integrity of the SRSF1 structure is required for efficient binding (**Fig. 1C**).

ABX300 modulates weight gain under a high-fat diet

To further study the effects of ABX300 on energy metabolism, DIO mice were treated with this compound by gavage, either subsequently or simultaneously to high-fat diet (HFD) condition. The average treatment length was one month, and the selected dose was 50 mg/Kg. This dose was the highest non-toxic dosage according to the maximal tolerated dose test in non-obese mice (**Fig. S2A**). In a curative context, ABX300 enhanced weight loss (**Fig. 2A**, left panel, day 34 *t-test p<0.0001, t=7.448, v=14*), reaching a plateau after 40 days of treatment (**Fig. S2B** left panel). ABX300 also prevented weight gain in normal mice receiving the HFD (**Fig. 2B**, left panel, day 34: *Mann-Whitney p=0.0002, U=0*). To assess whether the efficacy of the drug required the presence of fat and to assess this efficacy under standard diet conditions, mice receiving a chow diet (CD) were treated with ABX300. The weight and food intake of mice did not differ between groups (**Fig. 2C,** left panel, day34: *Mann-Whitney p=0.5072, U=102.5;* right panel: *Mann-Whitney p=0.4835, U=212*), demonstrating that ABX300 exerts its action only in obese mice or in lean mice under HFD.

However, a decrease in food intake was observed in DIO mice after only the five first days of treatment, and the amount of ingested food remained lower than in untreated animals over the period of treatment (**Fig. 2A** right panel, *Mann-Whitney p<0.001, U=17*). Cumulative food intake for the entire treatment period (shown at the bottom of the panels) significantly differed between treated and untreated animals. Nevertheless, the effects on body mass were stable and continuous (**Fig. S2B,** *Kruskal-Wallis followed by Dunn's post test p<0.0001*). To explore the contribution of reduced food intake to drug-

induced reductions in body weight, we performed a pair-feeding experiment. The amount of food eaten by the drug treatment group each day was determined, and this amount was provided to a vehicle-treated pair-fed group of animals housed under identical conditions the following day (**Fig. 2D** left panel, *day 30 ANOVA followed by Dunnet post test p<0.0001 between HFD untreated and HFD treated q=6.164 and p>0.05 between HFD untreated and Pair-fed q=1.644;, F=20.37*). **Fig. 2D** (right panel, *ANOVA followed by Dunnet post test p<0.05 between HFD untreated and HFD treated q=2.294 and p<0.05 HFD untreated and Pair-fed q=2.386; F=3.402*) shows that ABX300 treatment produced greater weight loss than that observed in the corresponding pair-fed group (left and right panels), implying that ABX300 treatment led to both reduced food intake and increased energy output. These effects are dose dependent because treatment of DIO mice with lower dose of ABX300 (20 mg/kg) did not induce any changes in food intake and weight compared to untreated mice (Fig.S2 B and C)

Importantly, no toxicity was observed in ABX300-treated animals following daily gavage. Up to 50 mg/kg, no significant weight loss was observed in lean mice treated compared to non treated mice (Fig.S2A) whereas in high fat diet-induced obese mice, treatment with ABX300 at 50 mg/kg decreased body weight (Fig.S2B). Histological examination confirmed the absence of toxicity but the loss of large adipocytes in the metabolic organs (WAT, BAT, liver and pancreas) and skin, between obese and obese mice treated for 65 days with ABX300 (Fig.S3 A and B). These results make unlikely the possibility that the weight loss is due tissue toxicity. Oral delivery of ABX300 did not change significantly the values of hematocrit (Fig.S2D, *Kruskal-Wallis followed by Dunn's post test p>0.05*) and lactate blood level was also similar between non treated and treated animals (Fig.S2E, *Kruskal-Wallis followed by Dunn's post test p>0.05*), revealing no hypoxic regions and no defect in liver clearance. Finally, no mark of inflammation was observed since blood resistin level did not change between treated and not treated animals (Fig.S2F, *Mann-Whitney p=0.0553, U=9*).

ABX300 decreases adiposity in DIO mice

The autopsy examination of adipose tissue showed a significant reduction in the WAT size in ABX300 DIO-treated mice compared with untreated mice (**Fig. S3A**). Specifically, the adipose mass was five times lower in treated mice, whereas the masses of all other organs remained constant (**Fig. 3A,** *Mann-Whitney p=0.0004, U=0*). To obtain a more comprehensive view of the fat distribution in these mice, we performed computed tomography. Based on an evaluation of both the subcutaneous and intra-abdominal adipose tissue volumes, all adipose tissue depots appeared to be equally affected by ABX300 treatment (**Fig. 3B**). The total fat volumes were calculated for each group, and ABX300 treatment was found to induce a 5.2-fold decrease in the adipose tissue volume compared with untreated mice (**Fig. 3C,** *Kruskall-Wallis followed by Dunn's post test p<0.01*). Remarkably, ABX300 DIO-treated mice were indistinguishable from untreated animals receiving a CD (**Fig. 3B and 3C**).

Hematoxylin-eosin (HE) staining of representative WAT, brown adipose tissue (BAT) and liver sections showed that ABX300 globally affected fat distribution. The treatment strongly reduced lipid accumulation in WAT (**Fig. 3D** and **Fig. S3A**), liver and BAT (**Fig. S3B**). In WAT, the quantification of the size of the adipocytes revealed that 80% of adipocytes in DIO-treated mice were small, (<2,000 µm²) whereas adipocytes size was heterogeneous in untreated mice, with 10% of the population exhibiting sizes larger than 10,000 µm² (**Fig. 3E,** <2000µm² *Mann-Whitney p=0.0079, U=0, v=5;* 2001<x<5000µm² *Mann-Whitney p=0.0159, U=1;* 5001<x<10000µm² *Mann-Whitney p=0.0079, U=0;* >10000µm² *Mann-Whitney p=0.0097, U=0*).

To verify whether enhanced lipolysis was involved in the observed effect of ABX300, we assessed glycerol, non-esterified fatty acids (NEFA) and triglycerides (TGs) in the serum of ABX300-treated and untreated animals. None of these parameters differed between the groups (**Fig. S3C**). While the treatment had no effect on glycemia **(Fig.S3E,** *Kruskall-Wallis followed by Dunn's post test p>0.05***),** it significantly enhanced the level of circulating Adiponetin **(Fig.S3D,** *Mann-Whitney p=0.012, U=4***)**. In addition, studies on differentiated adipocytes derived from the 3T3-L1 cell line (**Fig. S4A, S4B and 4C**), showed ABX300 treatment does not prevent differentiation or induce lipolysis.

Transcriptomic profiling of changes induced by ABX300

To analyze the profile program of AS changes occurring in the adipose tissue of treated and untreated DIO mice, we designed a large-scale screening strategy using high-throughput PCR on a pre-existing panel of 1,328 alternatively spliced events (ASEs) [20]. An analysis of the data allowed further stringent quality control measures; ASEs were only considered if >75% of the products ran at the expected motilities and if the total expected PCR concentration exceeded 20 nM. This filter ensured the use of high-quality PCRs for well-expressed genes and led to the use of 536 high-quality PCRs to conduct our adipose tissue analysis (**Table S1**). We used these high-quality PCRs to study the ASEs expressed in the WAT of ABX300-treated mice and compare them to untreated obese mice. The splicing profiles of pools of RNA extracted from 4 treated and 4 untreated WAT samples allowed the identification of 40 ASEs that varied by more than 20% between the two conditions (**Table S2**). Among the 40 selected ASEs, only 12 were reproducibly found in individual samples of each mouse (**Fig. 4A** and **Table S3**). Manual end-point PCRs are shown for the most robust changes in Myo9b02 and Pdlim5 (**Fig. 4B**). To test whether these splicing changes were affected by the HFD and/or ABX300 treatment, they were compared to the splicing profile in the adipose tissue from mice receiving a CD. **Figure 4B** shows that the splicing profiles of both Myo9b and Pdlim5 from CD mice were similar to the ones from DIO mice treated with ABX300, implying that the treatment reverses the splicing events altered by HFD and obesity.

Because variations in gene expression can also directly or indirectly contribute to the phenotype induced by ABX300, we used a dedicated qPCR array from QIAGEN SABiosciences; the Mouse Adipogenesis RT² Profiler™ PCR Array profiles the expression of 84 key genes involved in the differentiation and maintenance of mature adipocytes (Table S4). Among the 84 genes tested, 21 (25%) were significantly modulated in treated obese mice compared with untreated mice (**Fig. 4C,** *The p values are calculated based on a Student's t-test of the replicate 2^(- Delta Ct) values for each gene in the control group and treatment groups, and p values over than 0.05 are highlighted*). Most of these

transcriptional differences were also observed between DIO mice and CD mice (**Fig. 4D,** *The p values are calculated based on a Student's t-test of the replicate 2^(- Delta Ct) values for each gene in the control group and treatment groups, and p values over than 0.05 are highlighted*), suggesting that ABX300 treatment restores the transcriptional program modified by an HFD. The comparison between lean mice and treated obese mice confirmed this prediction. With the exception of Shh (Sonic Hedgehog) and Gata3 (Trans-acting T-cell-specific transcription factor GATA-3), which were up-regulated in treated DIO mice compared with CD untreated mice, all other transcripts perfectly correlated (**Fig. 4E,** *The p values are calculated based on a Student's t-test of the replicate 2^(- Delta Ct) values for each gene in the control group and treatment groups, and p values over than 0.05 are highlighted*). Again, this finding reinforced the notion that ABX300 restores the health of adipose tissue.

We next focused on expression of lamin A/C in obese and lean mice and found that both isoforms were downregulated specifically in WAT of obese mice but not in BAT, spleen and kidney (**Fig. S5A** and **S5B**). Interestingly, in ABX300-treated mice, both lamin A and lamin C were upregulated in WAT, BAT but also in kidney and liver (**Fig. S5C**, **S5D**, **S5E** and **S5F**). Again, this upregulation could be a marker of a healthy tissue.

ABX300 modulates the expression specific microRNAs

MicroRNAs (miRNAs) constitute a growing class of non-coding regulatory RNAs that primarily regulate gene expression by reducing mRNA stability and/or repressing translation [21]. Several miRNAs exhibit tissue-specific expression, and those present in WAT are known to have crucial implications for the regulatory networks underlying adipogenesis and adipose dysfunction in obesity [22]. The biogenesis of microRNA can be altered both at the transcriptional and post-transcriptional levels. SRSF1 recognizes the stem region of specific pri-miRNAs, resulting in enhanced cleavage by Drosha [23]. Furthermore, the microprocessor complex responsible for microRNA biogenesis was shown to competitively interact with the splicing machinery [24]. To assess the potential modulation of non-coding RNAs by ABX300

treatment, the population of miRNAs in the visceral WAT from HFD/CD untreated and ABX300-treated DIO mice was determined using Affymetrix microarrays. Among the 1,111 murine miRNAs that were analyzed, 52 were differentially expressed between untreated and treated animals (*Fold-change ≥1.5; P-value ≤0.05*). The heat map in **Figure 5A** shows the 26 up- and 26 down-regulated miRNAs (see also **Table S5**). Similarly, **Fig. 5B** and **Table S6** show the shifts of the 113 microRNAs (54 up-59 down regulated) varying between HFD and CD Untreated mice. Among the above mentioned variations, 37 of 52 (71%) miRNAs differentially expressed in HFD treated mice were found to have the same profile in CD mice (**Table S7**), corroborating the notion that ABX300 abolishes most changes in the biogenesis of miRNAs induced by an HFD. For instance, a hyper-caloric diet induced [25] while ABX300 treatment down-regulated the expression of miR-221, miR-222, miR-342-3p, and miR-146b (**Fig. 5A**). Conversely, miR-30c, miR-92a, miR-193b and miR-378 were decreased during obesity but up-regulated by ABX300 treatment (**Fig. 5A**). Furthermore, treating CD mice with ABX300 did not alter the expression of any microRNA except for miR-465c2, whose expression was significantly up-regulated 1.56-fold. This finding further suggests that ABX300 primarily modulates miRNA biogenesis in the context of an HFD (**Table S8**).

Interestingly, the expression levels of ten miRNAs varied exclusively in response to ABX300 but were not altered by diet: miR5122, miR5130, miR130b, miR199a-5p, miR362-5p, miR150-5p, miR26b-5p, miR714, miR92a, and miR29a. Eight of these ten microRNAs were predicted, based on a miRbase analysis (http://mirdb.org/ miRDB), to target mRNAs whose products are directly or indirectly involved in proper mitochondrial functioning (**Fig. 5C** and **Table S9**). This group of identified miRNAs represents a large fraction of all microRNAs mediating mitochondrial regulation, as only 16.47% of all microRNAs are expected to belong to this category (Mouse MitoCarta predicted 315 of 1,912). Among the eight identified microRNAs, miR-29a has been predicted to target Slc16a1 (**Table S9**), which plays a critical role in the regulation of energy balance when animals are exposed to an obesogenic diet [26]. Because each miRNA regulates, on average, approximately 200 target genes, ABX300 miR-specific

modulation most likely accounts for the observed phenotype.

ABX300 increases oxygen consumption

If ABX300 modulates the functioning of mitochondria, it is expected to generally impact the respiration of the entire organism. To assess respiration at the level of the whole animal, ABX300-treated and untreated mice were placed in metabolic cages. Oxygen consumption (VO_2) and CO_2 production (VCO_2) were monitored during a 12 h dark/ 12 h light cycle using the Oxymax Lab Animal Monitoring System (**Fig. 6A**). HFD ABX300-treated mice showed no differences in VO_2 and VCO_2 over a period of 24 h (**Fig. 6B,** *Mann-Whitney p=0.103, U=39)* and **Fig. 6C** right panels, *t-test p=0.943, t=0.072, ν=21*). However, when only focusing on the light period, i.e., the 8 h following ABX300 administration, treated DIO mice showed a marked tendency for higher O_2 consumption and CO_2 production compared with untreated DIO mice (**Fig. 6B** *Mann-Whitney p=0.001, U=12* and **Fig. 6C** left panels *t-test p=0.0376, t=2.219, ν=21).* These 8 h corresponded to the light period, when mice are normally at rest, and this period is characterized by a decrease in metabolism. These outcomes suggested that ABX300 treatment increased the basal metabolic rate of DIO mice. In addition, the respiratory exchange ratio (RER) was determined by calculating the VCO_2/VO_2 ratio. Likewise, ABX300-treated DIO mice demonstrated a RER close to 0.7, which indicates that fatty acids are the main metabolic source of energy. In contrast, untreated animals presented a RER ratio close to 0.8, showing a mixed consumption of fat and carbohydrates (**Fig. 6D** right panel**,** *t-test p=0.0130, t=2.714, ν=21*). These results indicate that ABX300 increases the metabolic rate, which results in the rapid metabolization of lipids, likely via mitochondrial β-oxidation.

Discussion

In this study, we developed a screening assay based on the AS regulation of the *LMNA* gene to identify ABX300, a compound that can bind SRSF1 *in vitro* and abrogates the effect of an HFD *in vivo*. Targeting splicing factors *in vivo* has not been tested mainly because these factors are ubiquitously expressed [27] and may have redundant functions in different tissues [28]. Nevertheless, previous studies have supported the relevance of AS isoforms in the regulation of metabolism [29]. Our data reinforce the idea that modulating the activity of splicing factors *in vivo* may impact RNA biogenesis in a more tissue-specific manner, providing opportunities for a new unexplored therapeutic approach for obesity. Although currently approved therapies for obesity focus on reducing caloric intake or blocking food absorption [30], changes induced by ABX300 favor EE. The effect of ABX300 appears to be mediated, at least in part, by changes in the expression of the *LMNA* gene and a subset of microRNAs involved in mitochondrial functioning.

The selectivity of ABX300 (weight loss exclusively under HFD conditions) (**Fig. 2**) pointed to a positive safety profile and further supported the possibility of developing ABX300 for therapeutic purposes. In addition to its influence on EE, ABX300 seemed to control feeding. However, a pair-feeding experiment demonstrated that reduced food intake alone was not sufficient to explain the observed phenotype (**Fig. 2D**). ABX300 can cross the blood brain barrier (Fig.S2G), presumably by transmembrane diffusion due to its solubility in lipid [31]. In the brain, ABX300 is unlikely to alter the AS of *LMNA* gene because *Lamin A* but not *Lamin C* transcripts are regulated by a specific microRNA miR-9 [32,33]leading to preferential expression of Lamin C in the brain. However, ABX300 might alter the biogenesis of microRNA involved in mitochondrial functioning in the brain like miR-29a which may target Slc16a1 to control the energy balance when animals are exposed to an obesogenic diet [26]. Another aspect of the safety profile of the drug is that ABX300 did not globally affect the AS of endogenous genes. Indeed, only a few of the AS events in the visceral WAT of treated animals were found to be altered by this molecule. Moreover, these changes suggested a return to normality because AS in

ABX300-treated mice returned to the profile of lean animals (**Fig. 4D**). Perhaps the most intriguing concept resulting from the findings presented herein is that small molecules targeting the core splicing machinery exert very small effects on different genes and alternative SS (**Fig. 4E**). Understanding the molecular basis of these differential effects may pave the way towards the rational design of compounds that can modulate the versatile effects of SS selection on gene expression [34,35]. SRSF1 can "travel" from the nucleus to the cytoplasm and is known to participate not only in the control of splicing and miRNA processing in the nucleus but also in the regulation of translation in the cytoplasm [27]. CLIP (cross-linking immunoprecipitation) experiments using anti-SRSF1-specific antibodies [36,37], splicing-sensitive RNA sequencing, microarray experiments [36] and polysomal fraction mRNAs analysis [38] have identified numerous potential "metabolic" targets for SRSF1, both at the splicing and the translational levels. Further studies focusing on the interaction of SRSF1 with other partners in the adipose tissue and how these factors are affected by HFD and ABX300 treatment would be of great utility for exploring the association of AS with metabolic alterations in obesity.

AS has also been described to affect microRNA biogenesis and regulation [39]. Splicing regulation *in vivo* may represent a system-wide response to the composition of miRNAs [40]. Nevertheless, how the impact on gene regulation by miRNAs will affect drug metabolism remains unknown [41]. In recent years, interest in the role of miRNAs in fat cell development and obesity has been rapidly growing. Understanding this role in the proliferation and differentiation of adipocytes during fat cell development may provide new therapeutic targets for anti-obesity drugs and early biomarkers for clinical diagnosis [22,42]. Moreover, miRNAs have been shown to play important roles in both brown and white fat differentiation [43] and in maintaining cell identity by fine-tuning cell-specific transcriptional networks [44]. In response to obesity, insulin resistance, or cold exposure, changes in miRNAs have been reported in adipose tissue [45]. These changes are consistent with our results, which indicate that ABX300 modulates mitochondrial microRNAs (**Fig. 5**), and seem to correlate with the observed phenotype of treated animals. Our data support the notion that targeting SRSF1 activity is a valid strategy to develop safe

anti-obesity drugs.

Acknowledgments

We are grateful to the Montpellier-RIO imaging platform (Montpellier, France), the Histology Experimental Network of Montpellier, and the IGMM animal facilities. The authors are grateful to Roscoe Klinck (Université de Sherbrooke), Pierre de la Grange (Genosplice), and Edouard Bertrand for the SRSF1-GFP HeLa cells. The screening reported in this paper was performed within the France-BioImaging national research infrastructure, at MRI, Montpellier. France-BioImaging is supported by the French National Research Agency through the ‘‘Investments for the Future’’ program (ANR-10-INSB-04). The authors thank Julien Bellis, Sylvain de Rossi and Virginie Georget for conducting the screening and microscopy imaging. We thank also Laurie Gayte for her help during the *in vivo* experiments.

Funding: This work was supported by the collaborative laboratory ABIVAX, OSEO-ISI CaReNA grant and Fondation pour la Recherche Médicale (FRM) grant (Equipe FRM 2011 -n°DEQ20111223745). JT is a senior member of the Institut Universitaire de France. CLH is an ESR fellow of the EU FP7 Marie Curie ITN RNPnet program (289007). ICLM was supported by a graduate fellowship from the Ministère Délégué à la Recherche et aux Technologies and CNRS.

Conflict of interest Statement : All the authors declare that these is no conflict of interest.

References

1 Van Gaal LF, Mertens IL, De Block CE. Mechanisms linking obesity with cardiovascular disease. *Nature* 2006; **444**: 875–880.

2 Ford ES, Giles WH, Dietz WH. Prevalence of the metabolic syndrome among US adults: findings from the third National Health and Nutrition Examination Survey. *JAMA* 2002; **287**: 356–359.

3 Saltiel AR. New therapeutic approaches for the treatment of obesity. *Sci Transl Med* 2016; **8**: 323rv2.

4 Spiegelman BM, Heinrich R. Biological control through regulated transcriptional coactivators. *Cell* 2004; **119**: 157–167.

5 Guan X-M, Chen H, Dobbelaar PH, Dong Y, Fong TM, Gagen K *et al.* Regulation of energy homeostasis by bombesin receptor subtype-3: selective receptor agonists for the treatment of obesity. *Cell Metab* 2010; **11**: 101–112.

6 Tseng Y-H, Cypess AM, Kahn CR. Cellular bioenergetics as a target for obesity therapy. *Nat Rev Drug Discov* 2010; **9**: 465–482.

7 Lopez-Mejia IC, De Toledo M, Chavey C, Lapasset L, Cavelier P, Lopez-Herrera C *et al.* Antagonistic functions of LMNA isoforms in energy expenditure and lifespan. *EMBO Rep* 2014; **15**: 529–539.

8 Worman HJ, Bonne G. 'Laminopathies': a wide spectrum of human diseases. *Exp Cell Res* 2007; **313**: 2121–2133.

9 Wilson KL, Zastrow MS, Lee KK. Lamins and disease: insights into nuclear infrastructure. *Cell* 2001; **104**: 647–650.

10 Navarro CL, Cau P, Lévy N. Molecular bases of progeroid syndromes. *Hum Mol Genet* 2006; **15 Spec No 2**: R151–61.

11 Eriksson M, Brown WT, Gordon LB, Glynn MW, Singer J, Scott L *et al.* Recurrent de novo point mutations in lamin A cause Hutchinson-Gilford progeria syndrome. *Nature* 2003; **423**: 293–298.

12 De Sandre-Giovannoli A, Bernard R, Cau P, Navarro C, Amiel J, Boccaccio I *et al.* Lamin a truncation in Hutchinson-Gilford progeria. *Science* 2003; **300**: 2055.

13 Arai Y, Takayama M, Abe Y, Hirose N. Adipokines and aging. *J Atheroscler Thromb* 2011; **18**: 545–550.

14 Lopez-Mejia IC, Vautrot V, De Toledo M, Behm-Ansmant I, Bourgeois CF, Navarro CL *et al.* A conserved splicing mechanism of the LMNA gene controls premature aging. *Hum Mol Genet* 2011; **20**: 4540–4555.

15 Vautrot V, Aigueperse C, Oillo-Blanloeil F, Hupont S, Stévenin J, Branlant C *et al.* Enhanced SRSF5 Protein Expression Reinforces Lamin A mRNA Production in HeLa Cells and Fibroblasts of Progeria Patients. *Hum Mutat* 2016; **37**: 280–291.

16 Tazi J, Bakkour N, Stamm S. Alternative splicing and disease. *Biochim Biophys Acta* 2009; **1792**:

14–26.

17 Soret J, Bakkour N, Maire S, Durand S, Zekri L, Gabut M *et al.* Selective modification of alternative splicing by indole derivatives that target serine-arginine-rich protein splicing factors. *Proc Natl Acad Sci USA* 2005; **102**: 8764–8769.

18 Bakkour N, Lin Y-L, Maire S, Ayadi L, Mahuteau-Betzer F, Nguyen CH *et al.* Small-molecule inhibition of HIV pre-mRNA splicing as a novel antiretroviral therapy to overcome drug resistance. *PLoS Pathog* 2007; **3**: 1530–1539.

19 Campos N, Myburgh R, Garcel A, Vautrin A, Lapasset L, Nadal ES *et al.* Long lasting control of viral rebound with a new drug ABX464 targeting Rev - mediated viral RNA biogenesis. *Retrovirology* 2015; **12**: 30.

20 Venables JP, Lapasset L, Gadea G, Fort P, Klinck R, Irimia M *et al.* MBNL1 and RBFOX2 cooperate to establish a splicing programme involved in pluripotent stem cell differentiation. *Nat Commun* 2013; **4**: 2480.

21 Makeyev EV, Maniatis T. Multilevel regulation of gene expression by microRNAs. *Science* 2008; **319**: 1789–1790.

22 McGregor RA, Choi MS. microRNAs in the regulation of adipogenesis and obesity. *Curr Mol Med* 2011; **11**: 304–316.

23 Wu H, Sun S, Tu K, Gao Y, Xie B, Krainer AR *et al.* A splicing-independent function of SF2/ASF in microRNA processing. *Mol Cell* 2010; **38**: 67–77.

24 Melamed Z, Levy A, Ashwal-Fluss R, Lev-Maor G, Mekahel K, Atias N *et al.* Alternative splicing regulates biogenesis of miRNAs located across exon-intron junctions. *Mol Cell* 2013; **50**: 869–881.

25 Ortega FJ, Moreno-Navarrete JM, Pardo G, Sabater M, Hummel M, Ferrer A *et al.* MiRNA expression profile of human subcutaneous adipose and during adipocyte differentiation. *PLoS ONE* 2010; **5**: e9022.

26 Lengacher S, Nehiri-Sitayeb T, Steiner N, Carneiro L, Favrod C, Preitner F *et al.* Resistance to diet-induced obesity and associated metabolic perturbations in haploinsufficient monocarboxylate transporter 1 mice. *PLoS ONE* 2013; **8**: e82505.

27 Cáceres JF, Screaton GR, Krainer AR. A specific subset of SR proteins shuttles continuously between the nucleus and the cytoplasm. *Genes Dev* 1998; **12**: 55–66.

28 Longman D, Johnstone IL, Cáceres JF. Functional characterization of SR and SR-related genes in Caenorhabditis elegans. *EMBO J* 2000; **19**: 1625–1637.

29 Li H, Cheng Y, Wu W, Liu Y, Wei N, Feng X *et al.* SRSF10 regulates alternative splicing and is required for adipocyte differentiation. *Mol Cell Biol* 2014; **34**: 2198–2207.

30 Jackson VM, Breen DM, Fortin J-P, Liou A, Kuzmiski JB, Loomis AK *et al.* Latest approaches for the treatment of obesity. *Expert Opin Drug Discov* 2015; **10**: 825–839.

31 Lipid solubility and drug penetration of the blood brain barrier. 1974; **147**: 813–815.

32 Jung H-J, Coffinier C, Choe Y, Beigneux AP, Davies BSJ, Yang SH *et al.* Regulation of prelamin A but not lamin C by miR-9, a brain-specific microRNA. *Proc Natl Acad Sci USA* 2012; **109**: E423–31.

33 Nissan X, Blondel S, Navarro C, Maury Y, Denis C, Girard M *et al.* Unique preservation of neural cells in Hutchinson- Gilford progeria syndrome is due to the expression of the neural-specific miR-9 microRNA. *Cell Rep* 2012; **2**: 1–9.

34 Tazi J, Durand S, Jeanteur P. The spliceosome: a novel multi-faceted target for therapy. *Trends Biochem Sci* 2005; **30**: 469–478.

35 Bonnal S, Vigevani L, Valcárcel J. The spliceosome as a target of novel antitumour drugs. *Nat Rev Drug Discov* 2012; **11**: 847–859.

36 Pandit S, Zhou Y, Shiue L, Coutinho-Mansfield G, Li H, Qiu J *et al.* Genome-wide analysis reveals SR protein cooperation and competition in regulated splicing. *Mol Cell* 2013; **50**: 223–235.

37 Sanford JR, Coutinho P, Hackett JA, Wang X, Ranahan W, Cáceres JF. Identification of nuclear and cytoplasmic mRNA targets for the shuttling protein SF2/ASF. *PLoS ONE* 2008; **3**: e3369.

38 Maslon MM, Heras SR, Bellora N, Eyras E, Cáceres JF. The translational landscape of the splicing factor SRSF1 and its role in mitosis. *Elife* 2014; : e02028.

39 Passetti F, Ferreira CG, Costa FF. The impact of microRNAs and alternative splicing in pharmacogenomics. *Pharmacogenomics J* 2009; **9**: 1–13.

40 Fu X-D, Ares M. Context-dependent control of alternative splicing by RNA-binding proteins. *Nat Rev Genet* 2014; **15**: 689–701.

41 Kwan T, Benovoy D, Dias C, Gurd S, Provencher C, Beaulieu P *et al.* Genome-wide analysis of transcript isoform variation in humans. *Nat Genet* 2008; **40**: 225–231.

42 Heneghan HM, Miller N, Kerin MJ. Role of microRNAs in obesity and the metabolic syndrome. *Obes Rev* 2010; **11**: 354–361.

43 Mori MA, Thomou T, Boucher J, Lee KY, Lallukka S, Kim JK *et al.* Altered miRNA processing disrupts brown/white adipocyte determination and associates with lipodystrophy. *J Clin Invest* 2014; **124**: 3339–3351.

44 Ebert MS, Sharp PA. Roles for microRNAs in conferring robustness to biological processes. *Cell* 2012; **149**: 515–524.

45 Mori M, Nakagami H, Rodriguez-Araujo G, Nimura K, Kaneda Y. Essential role for miR-196a in brown adipogenesis of white fat progenitor cells. *PLoS Biol* 2012; **10**: e1001314.

Figures Legends

Figure 1: Identification of ABX300 as a SRSF1 partner that modulates LMNA splicing.

(**A**) Effect of selected drugs on the localization of SRSF1 in CRISPR-edited HeLa cells expressing an endogenous GFP-SRSF1without treatment (DMSO) treated with ABX300 (ABX 300) or positive control ABX 460 (ABX460). Nuclei visualized with Hoecht staining (Hoecht) and SRSF1 localization by GFP (SRSF1-GFP). (**B**) Schematic representation of *in vitro* screening based on the LMNA-Luc splicing reporter. The position of exon, intron and splice sites are shown.

(**C**) Fluorimetric titration of SRSF1 with ABX300 at 1.2 µM. Error bar indicates +/- SD.

Figure 2: ABX300 treatment blocks HFD-induced obesity in mice.

(**A**) Monitoring of body weight changes (left panel) and the average daily (right panel) and cumulative food intakes (histogram under the curve) of untreated and treated DIO animals in a curative context. Error bar indicates +/- SEM (n=8 for each groups). (**B**) Monitoring of body weight changes (left panel) and average daily (right panel) and cumulative food intakes (histogram under the curve) of untreated and treated animals in a preventive context. Error bar indicates +/- SEM (n=10 for each groups). (**C**) Monitoring of body weight changes (left panel) and average daily and cumulative food intakes (right panel) of untreated and treated animals under normal CD conditions (n=11 for each groups). Error bar indicates +/- SEM. (**D**) Effect of caloric restriction on body weight (left panel) and average daily and cumulative food intakes (right panel) in DIO animals. Error bar indicates +/- SEM (n=9 for each groups).

Figure 3: ABX300 decreases adiposity in DIO mice.

(**A**) Weights of individual organs after 35 days of treatment shown as the fold-change compared with the untreated group. Error bar indicates +/- SEM (HFD untreated n=9, HFD treated n=6). (**B**) Representative

PET-CT imaging for HFD untreated, HFD treated and CD untreated mice. (**C**) Quantification of fat tissue volume (expressed in mm^3) by PET-CT scan analysis (HFD untreated n=9, HFD treated n=4 and CD untreated n=10). (**D**) Representative images of HE-stained sections of the WAT from HFD untreated and HFD treated mice. (**E**) Quantification of adipocytes by size from the WAT of HFD untreated and HFD treated mice (expressed in % of lipids droplets per size range, n=5 for each groups). Error bar indicates +/- SEM.

Figure 4: Effect of ABX300 on the splicing and transcriptome of genes involved in adipose tissue homeostasis.

(**A**) Schematic representation of the selection process of ASE and a heat map of the 12 most relevant genes. (**B**) Expression of Myo9_e02 and Pdlim2 by PCR in obese treated/untreated mice compared with lean mice. (**C**) Scatter plot comparing HFD treated mice with HFD untreated mice showing up-regulated and down-regulated genes. (**D**) Scatter plot comparing CD untreated mice and HFD untreated mice. (**E**) Scatter plot comparing CD untreated mice and HFD treated mice.

Figure 5: ABX300 modulates mitochondrial targeted microRNAs

(A) Heat map showing upregulation (red) and dowregulation (green) of 52 micro-RNA between HFD untreated and treated animals one month after drug administration. (**B**) Heat map showing upregulation (red) and dowregulation (green) of 113 micro-RNA between HFD untreated and CD untreated animals one month after drug administration. (**C**) The Venn diagram shows the number of shared and unique miRNAs expressed in response to different diet and treatment conditions. The circumference of the overlapping area refers to the 42 miRNAs whose expression levels reverted to the lean level, i.e., that in healthy WAT, after ABX300 treatment and were are up-regulated (red) or down-regulated (green) in HFD untreated when compared to CD untreated (green circle) or HFD treated (blue circle) mice. The fold-changes and P-values of individual miRNAs are summarized in Supplementary Tables S5, S6, S7

and S8.

Figure 6: ABX300 increases oxygen consumption.

(A) Monitoring of VO_2 consumption (left panel) and CO_2 production (right panel) over a period of 24 h (12 h-light / 12 h-dark) in HFD untreated (n=12) and HFD treated mice (n=11). Values are normalized to body weight (**B**) Mean of VO_2 consumption 8 h after treatment (left panel) and 24 h after treatment (right panel). Error bar indicates Min. to Max. (**C**) Mean of CO_2 production 8 h after treatment (left panel) and 24 h after treatment (right panel). Error bar indicates Min to Max. (**D**) Respiratory exchange ratio (RER) 8 h after treatment (left panel) and 24 h after treatment (right panel). Error bar indicates Min. to Max.

Fig. 1

A

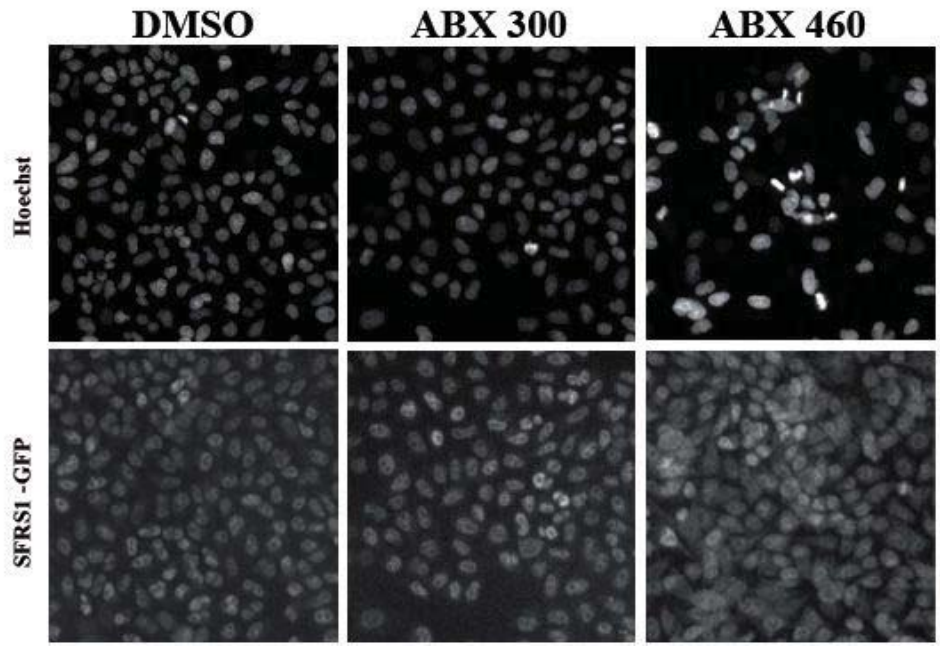

B

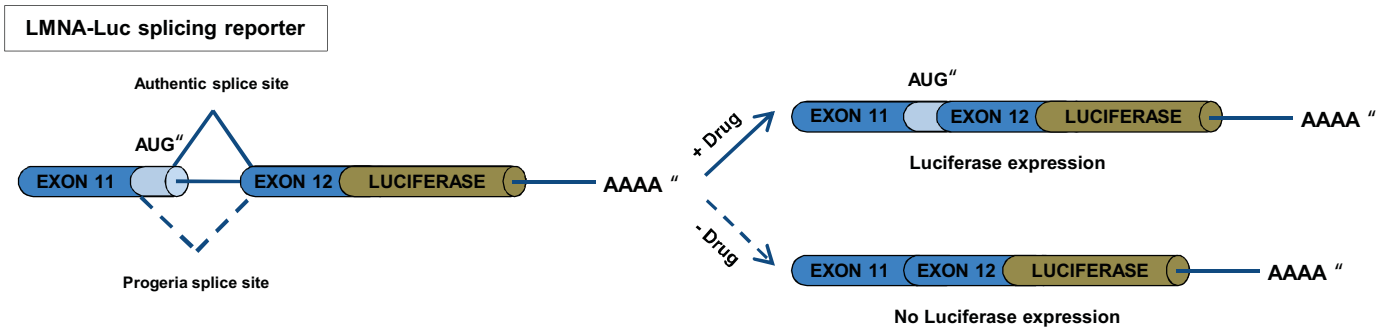

C

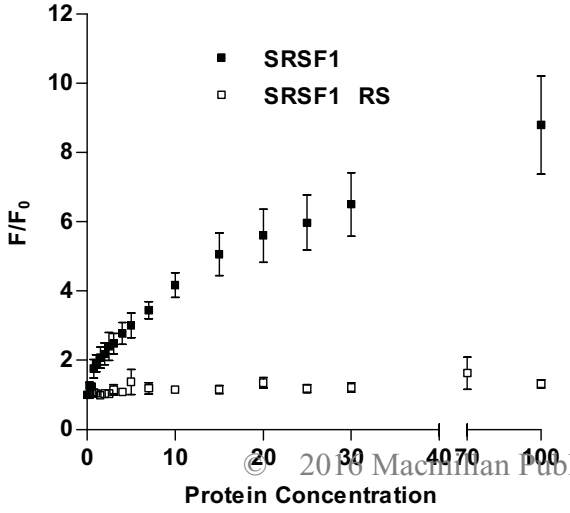

Fig. 2

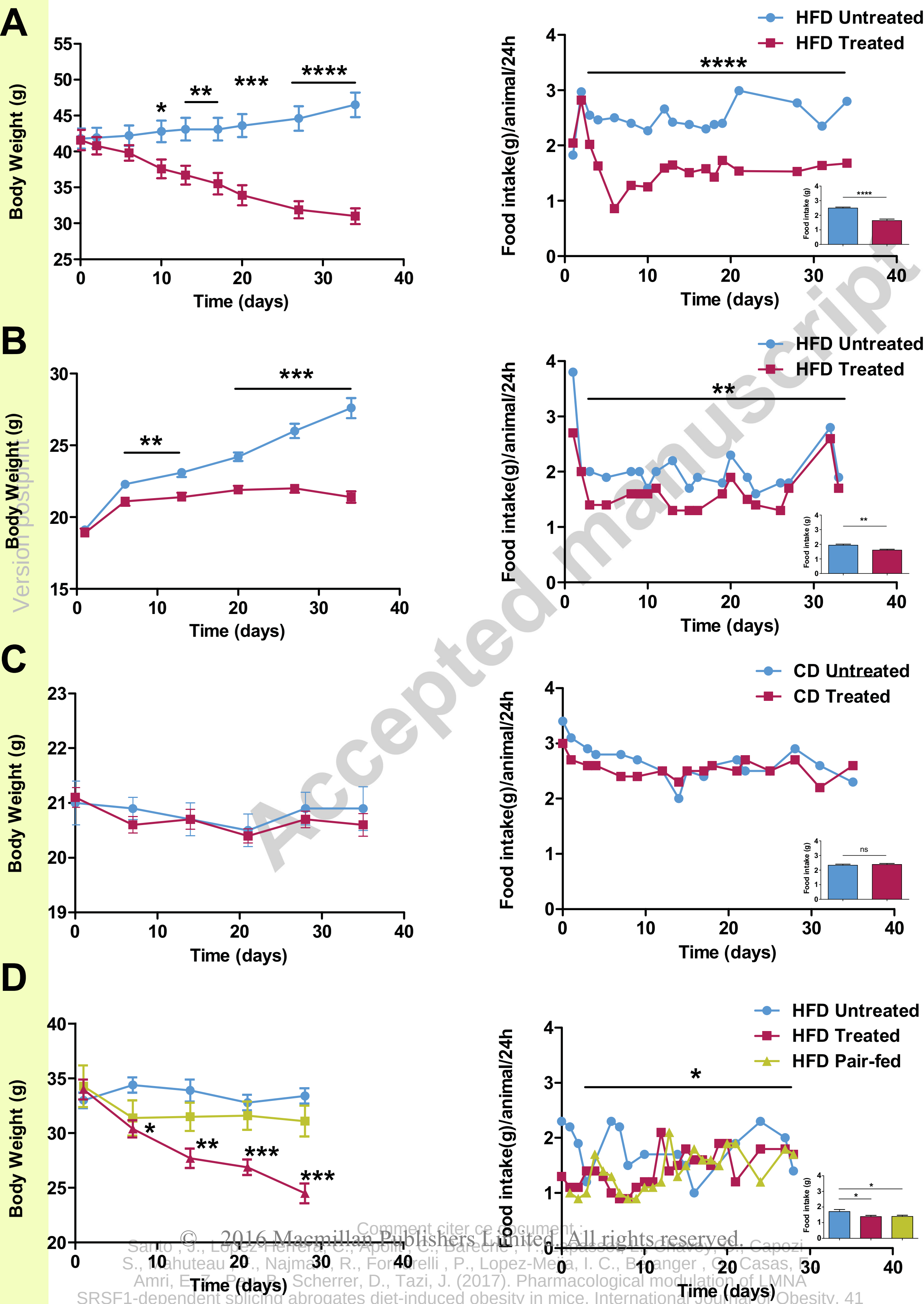

Fig. 3

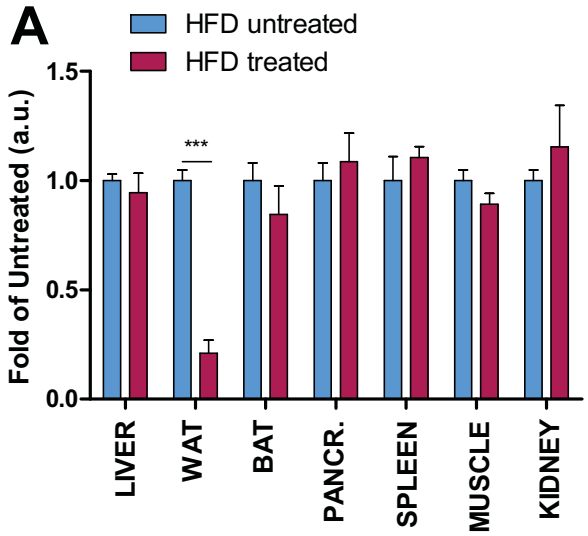

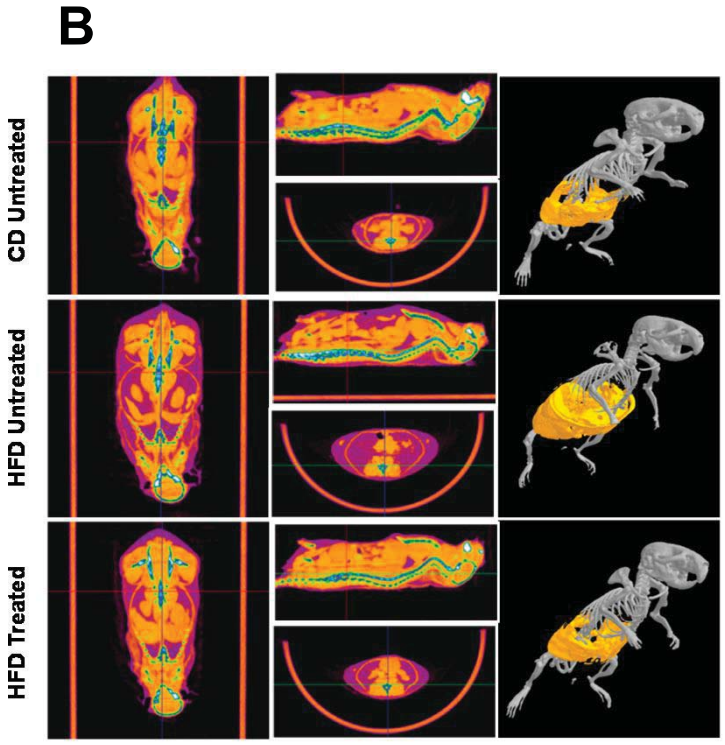

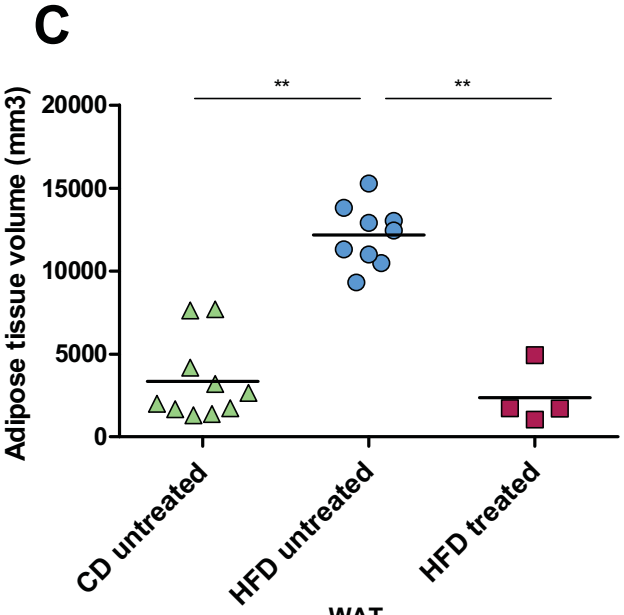

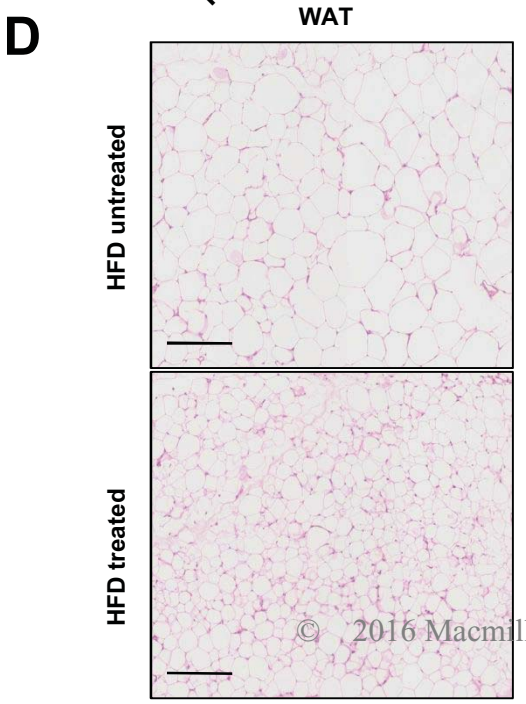

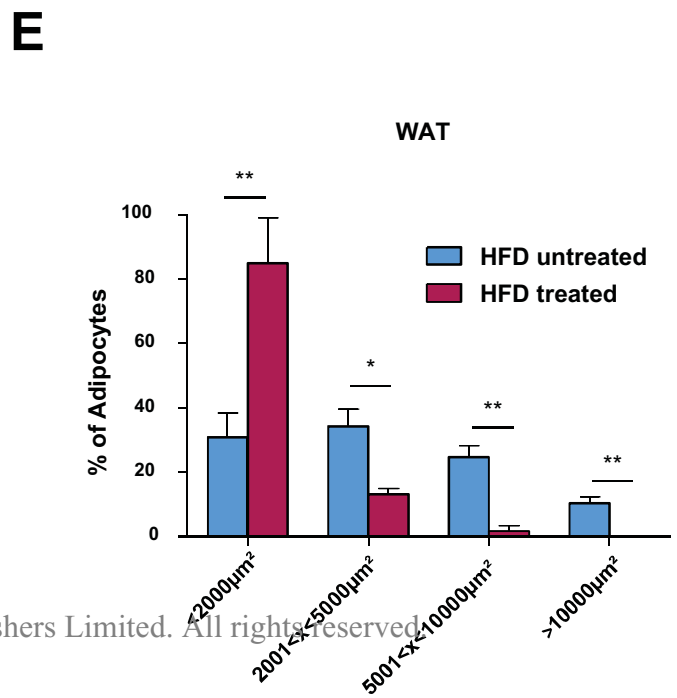

Fig.4

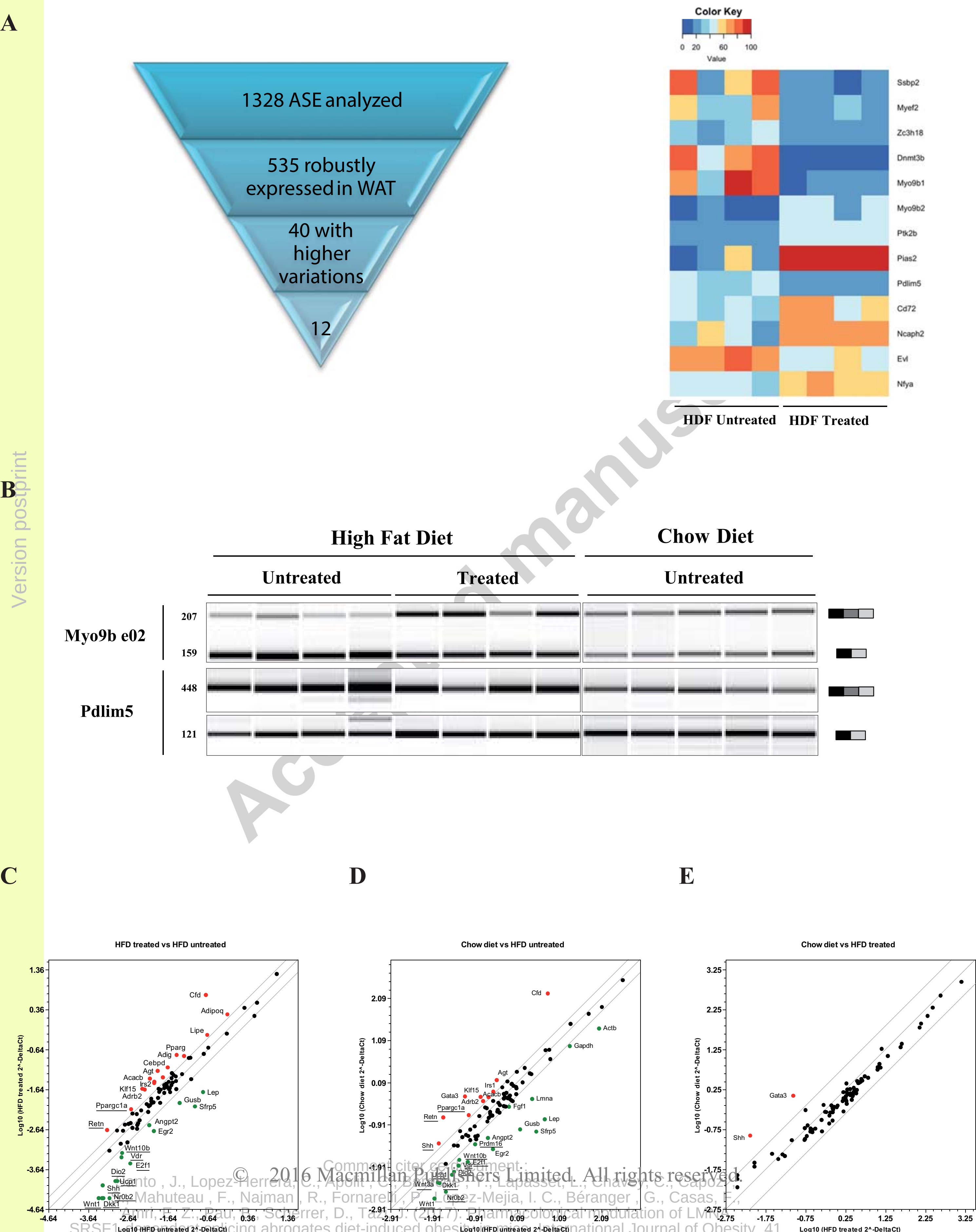

Fig. 5

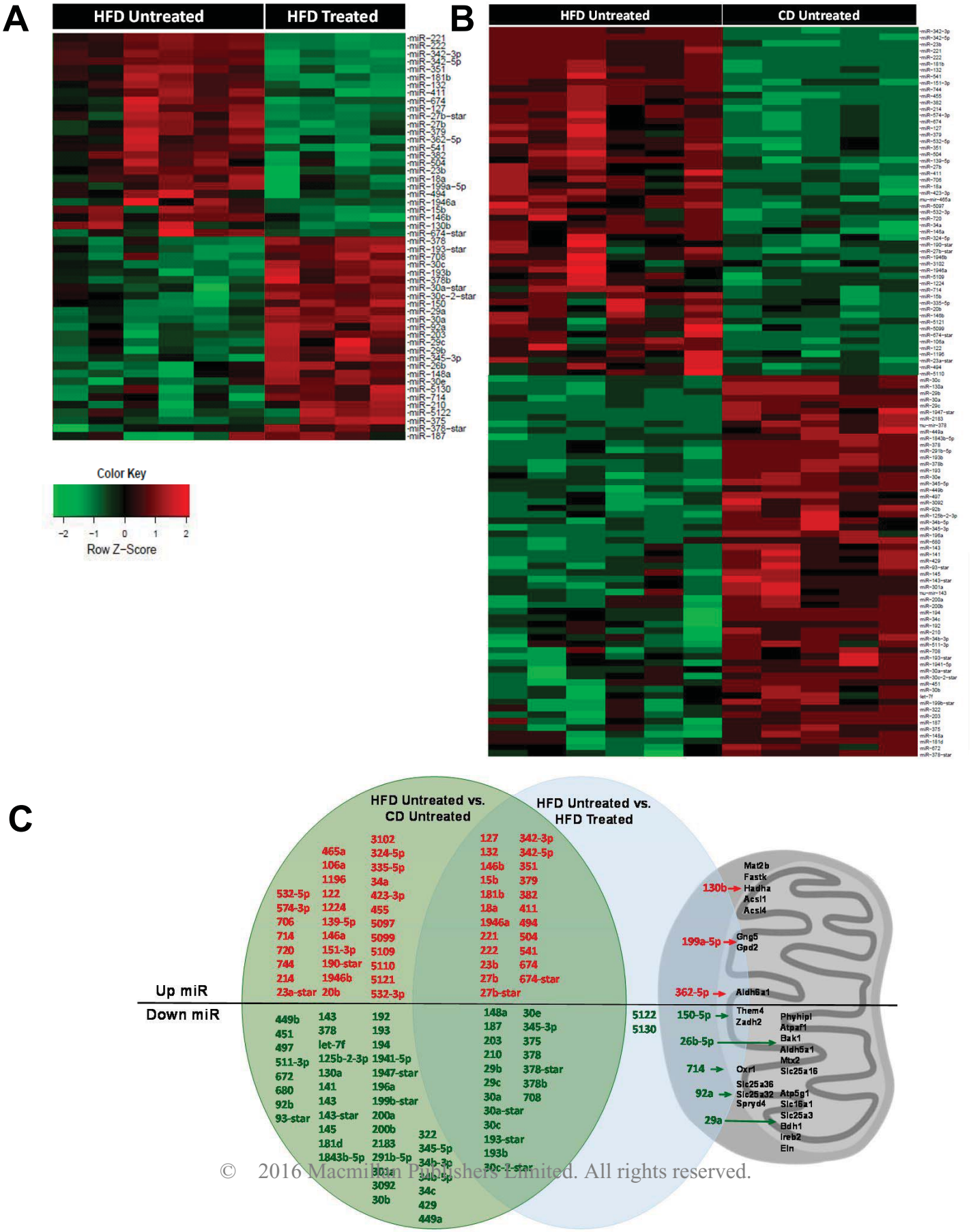

Fig. 6